Research Article | Vol. 32, No. 8 / 8 Apr 2024 / Optics Express 13965
Optics EXPRESS

Control of light polarization by optically-induced-chirality in photosensitive nematic fluids

LUGUO HAO,[1] FEI LIANG,[1] HONGZHEN JING,[1] YING XIANG,[1,6] PÉTER SALAMON,[2,7] NÁNDOR ÉBER,[2] ÁGNES BUKA,[2] MICHAL KOHOUT,[3] JIAWEN CHEN,[4] AND YANBO PEI[5]

[1]*School of Information Engineering, Guangdong University of Technology, Guangzhou 510006, China*
[2]*HUN-REN Wigner Research Centre for Physics, 1525 Budapest, P.O. Box 49, Hungary*
[3]*Department of Organic Chemistry, University of Chemistry and Technology Prague, Technická 5, CZ-16628 Prague, Czech Republic*
[4]*National Center for International Research on Green Optoelectronics, South China Normal University, Guangzhou 510006, China*
[5]*School of Physics, Harbin Institute of Technology, Harbin 150000, China*
[6]*frank_xiang68@qq.com*
[7]*salamon.peter@wigner.hun-ren.hu*

Abstract: Light polarization rotations, created by applied optical field, are examined experimentally and theoretically in a photosensitive chiral nematic fluid. The polarization rotation of the transmitted beam is initiated by illuminating the sample with uniform UV light. The operation is tunable and reversible, depending on the UV intensity. It was revealed that the rotations can be ascribed to the optical-field-induced chirality effect, where the helical structure in chiral nematics changes in accordance with the UV intensity. The evolution of the helical structure as well as its effect on the light polarization upon illumination by uniform UV light have been monitored experimentally and compared by calculations based on the continuum theory. Our results proved that a polarization field with specific characteristics can be achieved using the remote and precise optical control.

1. Introduction

Apart from the intensity, frequency and phase, polarization is another important characteristic of light, which has recently extensively been concerned in the fields of optical communication, polarization imaging, biomedical analysis and materials characterization.

Some materials, such as azobenzenes or dichroic dyes, are capable of giving photosensitive response to the light polarization, which can be exploited in photonic devices to perform specific functionalities associated with polarization field [1,2]. Besides, thanks to the optical anisotropy and sensitivity to the external fields, nematics are also ideal candidates to tune the polarization state of transmitted light [3]. One famous example is the twisted nematic device, where the director rotates along a helical axis; with such a structure the electric vector of transmitted light follows the rotation of the director synchronously and the corresponding polarization state changes accordingly [4–6]. Another well-known example is an optical waveplate with desired retardation, which transforms the polarization state due to birefringence [7,8]. In the above-mentioned cases, the direction and magnitude of the polarization variation is determined by the surface alignments and the (induced) helical pitch of nematics; thus, they both are static and fixed during the device preparation, which brings about rather an inflexibility in application [9].

In order to manipulate the light polarization dynamically, recently a new system composed of a nematic and a photosensitive chiral dopant has been introduced [10]. As the helical twisting

#522820 https://doi.org/10.1364/OE.522820
Journal © 2024 Received 4 Mar 2024; revised 18 Mar 2024; accepted 18 Mar 2024; published 1 Apr 2024

Optics EXPRESS

power (*HTP*) of our chiral dopant changes upon illumination by UV light, the induced helical structure of the system, as well as the orientation of the applied voltage induced electroconvection patterns can be controlled by the UV field [11]. Adopting a hybrid aligned cell (HAC) geometry to ensure the change of helical pitch freely, the change of pattern orientation could be made continuous, facilitating a two-dimensional beam steering [12].

In this paper, we show that the HAC system above is also capable of rotating the polarization state of transmitted light using a controlling UV field. We demonstrate an unusual linear polarization rotator, which is able to dynamically and continuously twist the plane of a linearly polarized light and can be tuned optically. It is anticipated that such effects can be generalized to fabricate fantastic photonic devices, such as polarization rotator arrays, which can define spatial polarization distributions according to custom presetting, with dynamically and in situ switchable tunability.

We are aware that the method described in this paper is not the only possibility to realize continuous polarization rotation. Recently, an alternative way with slightly different geometry (tangential – conical boundary conditions) has also been proposed to perform such operations [13]. In addition, recently a conceptionally different technique based on heliconical cholesterics with short pitch ($P \sim \lambda$) has also been suggested to achieve continuous polarization rotations [14,15]. Our method works in a completely different pitch range ($P >> \lambda$) of the light transmission, where the Mauguin limit fulfils. In addition, the optical tuning is not based on the optical torque as in the heliconical case, but rather on the molecular conformation changes induced by the illuminating UV light.

2. Materials and methods

2.1. Samples

The measurements were performed on a cholesteric liquid crystal (CLC) obtained by doping the nematic host E7 with the chiral dopant M5(R) (9-(2-methyl-2,3-dihydro-1H-cyclopenta[a]naphthalen-1-ylidene)-9H-fluorene) at weight concentration C_{M5}. The CLC compound was filled into hybrid aligned cells with thickness d, where one substrate surface was treated by the polyimide (PI) Nissan 7511 L to obtain homeotropic alignment, while the other substrate was covered by the PI Nissan SE150, which resulted in a parallel alignment after rubbing along the direction $\mathbf{n}_0$.

As a photosensitive molecular switch (also called as light powered nanomotor [16]), the *HTP* of the chiral dopant M5(R) varies with the intensity of UV irradiation, resulting in a tunable helical pitch $P(I_{uv})$ [10,11,17]. It was found that there is a critical UV intensity $I_c = 1.25$ mWcm^{-2}, where the *HTP* becomes zero, i.e. the helical structure fully unwinds yielding a nematic-like, compensated cholesteric state with $|P(I_c)| = \infty$. Initially, without UV illumination, the dopant M5(R) induced *right-handed* cholesteric helix; afterwards, upon UV illuminating, M5(R) molecules may undergo photoisomerisation; if the UV intensity exceeds I_c, then the helix switches to an opposite (*left-handed*) helical sense [12].

2.2. Photo-tuning setup

A DMD (digital micro-mirror device) - based dynamic mask photo-tuning technique was employed, where a collimated $\lambda = 365$ nm UV beam from a LED lighter (FUV-8BIT, Height-LED Opto-electronics Technology Co.), acting as command light, was reflected onto the DMD and subsequently carried a designed light intensity pattern (Fig. 1). In our experiments, a uniform (pattern free) image was uploaded into the DMD producing homogeneous UV intensity I_{uv}, which could be adjusted by the grey level of the image.

After being focused by an objective, the UV beam was projected onto the sample, whose intensity was detected by an UV meter (UV-A from Bejing Shida Photoelectric Technology) placed in front of sample. A linearly polarized laser (λ=633 nm) acted as probe beam and

Optics EXPRESS

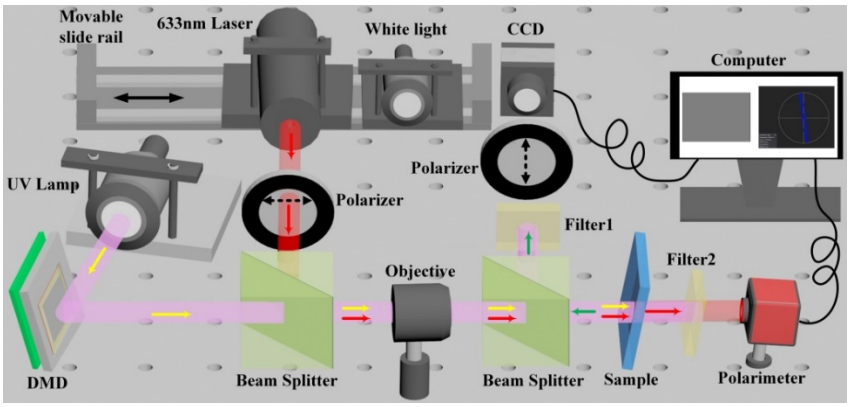

Fig. 1. Schematic diagram of the DMD-based dynamic mask system for photo-tuning, which integrated light emission, dynamic pattern generation, image focusing and monitor components.

impinged upon the sample, and the polarization state of transmitted beam was measured by a polarimeter (PAX1000 from THORLABS). Besides, in order to check how morphologies of the sample changed with varying I_{uv}, the 633 nm laser beam was replaced by a collimated white light, with the help of front and rear polarizers, colorful optical textures were monitored by a CCD at reflected-light mode [18]. Meanwhile, two optical color filters were installed before the polarimeter and CCD to block the UV light, respectively.

3. Experimental results

In the following experiments, samples with $C_{M5} = 0.0075\%$ and $d = 60\,\mu m$ were inspected typically, where the combination of the values of C_{M5} and d were selected so that to produce a $\pi/2$ rotation of transmitted light's polarization at I_{uv} =0 with respect to that of the incident beam. At this concentration the initial (unilluminated) pitch is $P_0 = 2.13 \cdot d = 128\,\mu m$. A uniform UV field was used to tune the pitch and to manipulate the polarization states of the transmitted beam.

3.1. Polarization rotation of the transmitted beam

When subjected to a controlling UV light, both the pitch P and the chirality of samples changed accordingly. For the spatially uniform I_{uv}, the corresponding helical structure distributed homogeneously in the whole sample.

Depending on I_{uv}, four kinds of helical structures appeared, demonstrated in Figs. 2(a)–2(d), respectively: ① initially *right-handed* state with $P_0 > 0$ at I_{uv} =0; ② *right-handed* states with $P(I_{uv}) > P_0 > 0$ in the range of $0 < I_{uv} < I_c$; ③ *unwound, compensated state* with $P(I_c) \approx \infty$ at $I_{uv} = I_c$; ④ *left-handed* states with $P(I_{uv}) < 0$ in the range of $I_c < I_{uv}$, indicating a handedness inversion.

As the helical structure was homogeneous in the cell plane, the normally incident light beam travelled through the sample directly. Due to the interaction between the helical structure and the incident beam, characteristics of the transmitted beam, such as the polarization state and the output intensity, may differ from that of the incident beam, as shown in Fig. 3. In the following, we demonstrate how a uniform I_{uv} affects the sample, its polarization state and the output intensity of the transmitted light.

Optics EXPRESS

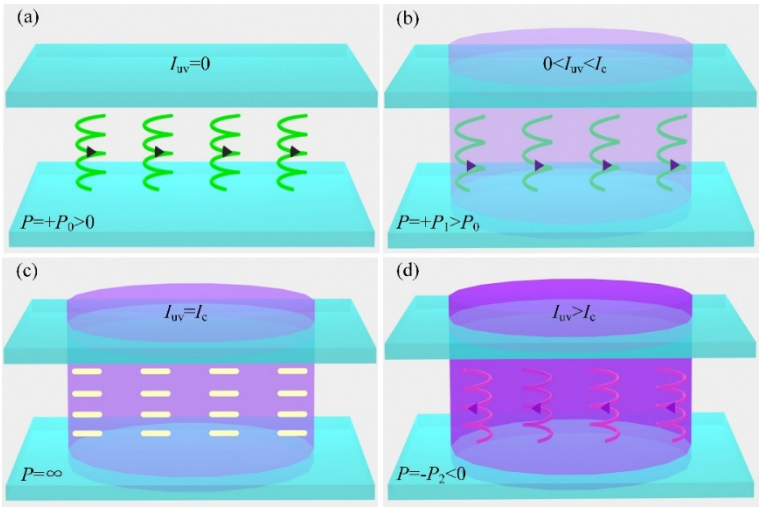

Fig. 2. Schematic illustration of the evolution of helical structures upon illumination by a uniform UV light with intensity I_{uv}, where (a) the sample stays in its initially right-handed state with pitch + P_0 at I_{uv} =0; (b) the sample remains in a right-handed state with pitch + P_1 ($|P_1|>|P_0|$), when $I_{uv} < I_c$; (c) the sample becomes compensated with pitch $|P| = \infty$ at $I_{uv} = I_c$; (d) the sample turns into a left-handed state with pitch of -P_2, when $I_{uv} > I_c$.

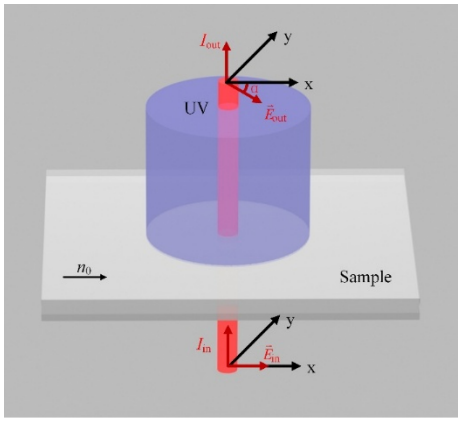

Fig. 3. Schematic diagram of light traveling through a sample, illuminated by an additional uniform UV light. I_{in} and E_{in}, I_{out} and E_{out} are the intensity and polarization state of the incident and the transmitted beam, respectively.

Optics EXPRESS

3.2. Dependence of the CLC texture upon the UV intensity

Illuminated by uniform I_{uv}, various excited, pattern-free states were formed in the samples with crossed polarizers, characterized by different colors. It should be noted that upon enhancing I_{uv}, the resulting colors changed smoothly: at $0 \le I_{uv} \le I_c$, the samples changed from the initial bright texture (Fig. 4(a)) to a dim texture (Fig. 4(b)), then an extinction texture corresponding to the unwound, compensated state with $P(I_c) \approx \infty$ in Fig. 4(c); afterwards, when $I_c \le I_{uv}$, the samples went through the above states with reversed handedness, as shown in Figs. 4(d) - 4(f).

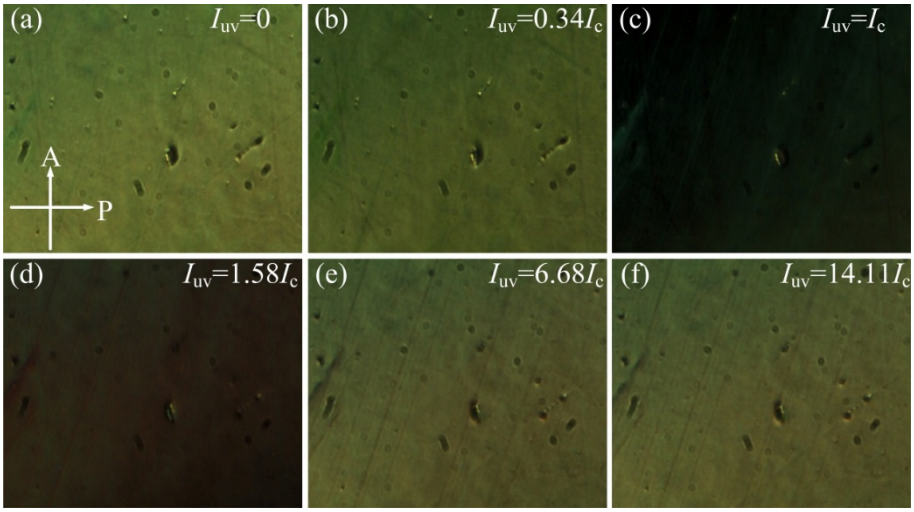

Fig. 4. Representative optical textures (450 μm × 290 μm) at crossed polarizer P and analyzer A, illuminated by increasing uniform UV intensity, where (a) $I_{uv} = 0$, (b) $I_{uv} = 0.34$ I_c, (c) $I_{uv} = 1.0$ I_c, (d) $I_{uv} = 1.58$ I_c, (e) $I_{uv} = 6.68$ I_c and (f) $I_{uv} = 14.1$ I_c, respectively.

3.3. Dependence of the polarization state upon the UV intensity

When the incident beam was linearly polarized with polarization along the x axis (azimuth angle of the polarization: $\alpha = 0$), it was observed that during the change of I_{uv}, the polarization state of the transmitted beam was almost linear, while the polarization angle α varied, as illustrated in Fig. 5.

Further inspection indicated that for the *initially right-handed* sample, upon enhancing I_{uv}, α decreased monotonically and continuously by rotating clockwise, even when the sample had turned into a *left-handed* one due to $I_{uv} > I_c$. Eventually, α could be adjusted between -π/2 and +π/2, thus the polarization state can sweep the whole plane, as shown in Fig. 5 and Fig. 6(a).

3.4. Degree of polarization of the transmitted beam versus the UV intensity

The variation of the degree of linear polarization (*DoLP*) of the transmitted beam was examined depending on the I_{uv}, as shown in Fig. 6(b). Herein, *DoLP* was defined as $DoLP = I_{major}/(I_{major} + I_{minor})$, where I_{major} and I_{minor} are the intensities along the major and the minor axes of the elliptically polarized beam, respectively. $DoLP = 1$ means a perfectly linearly polarized state.

It was found that the *DoLP* indicates a reasonably high degree of linear light polarization during the whole adjustability range of $-\pi/2 \le \alpha \le +\pi/2$.

Optics EXPRESS

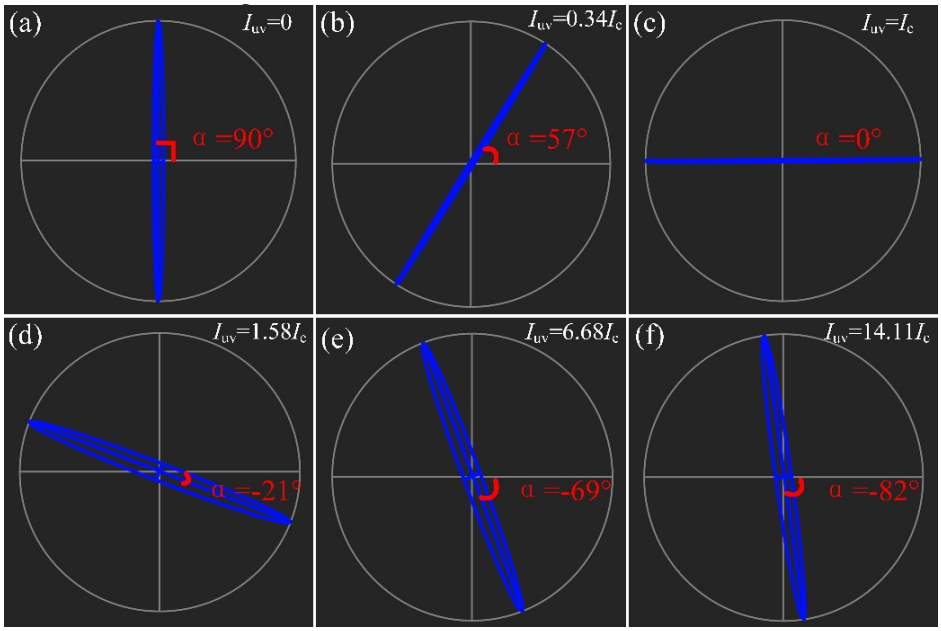

Fig. 5. Representative polarization states of the transmitted beam upon uniform UV field with (a) $I_{uv} = 0$, (b) $I_{uv} = 0.34\ I_c$, (c) $I_{uv} = 1.0\ I_c$, (d) $I_{uv} = 1.58\ I_c$, (e) $I_{uv} = 6.68\ I_c$ and (f) $I_{uv} = 14.1\ I_c$, respectively; α is the polarization angle.

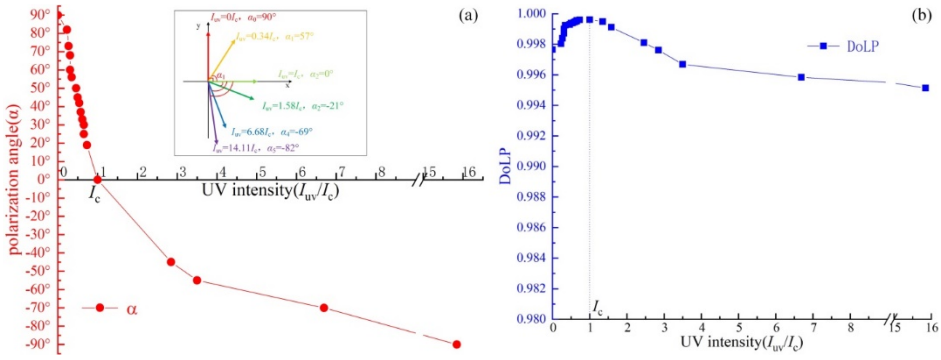

Fig. 6. Dependence of (a) the polarization angle α and (b) the degree of linear polarization (*DoLP*) of the transmitted beam on the UV intensity I_{uv}. The inset illustrates the rotation of the polarization state with increasing I_{uv} in the initially right-handed sample.

Optics EXPRESS

3.5. Effect of the sample thickness on the photo-tuning operation

It was found that the thickness d is a critical factor to determine the photo-tuning results, as shown in Fig. 7. Three samples were prepared and compared, where the dopant concentration C_{M5} and thickness d were carefully combined in order to fix $\alpha = \pi/2$ for the transmitted beam at the initial unperturbed state ($I_{uv} = 0$).

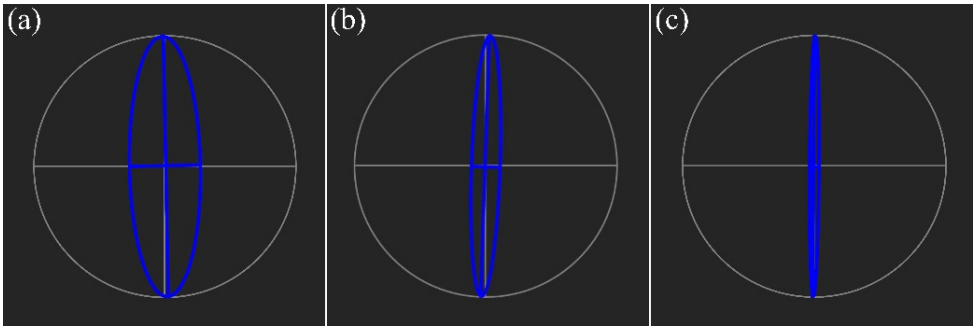

Fig. 7. Dependence of the polarization state of the transmitted beam on the cell thickness d at $I_{uv} = 0$. The representative thicknesses d (C_{M5}) are (a) 9 µm (0.06%), (b) 36 µm (0.013%), (c) 60 µm (0.0075%).

Under such conditions, the polarization state of the transmitted beam in the absence of UV illumination varies significantly with d; namely, a larger d induces a higher *DoLP* (reduction of the ellipticity), as illustrated in Fig. 7.

4. Discussion

As the characteristics of the transmitted beam closely correlate with the pitch P of the sample, the knowledge of how P is modulated by the UV light is a precondition for understanding the tunability mechanism.

4.1. Calculation of the director field in the hybrid aligned cholesteric sample

The director field in the HAC geometry can be calculated from the continuum theory [3,19]. The director field is represented by the tilt angle ϑ and the azimuthal angle φ. It is assumed that the director is homogeneous in the x-y plane, i.e. both angles depend on the coordinate z (normal to the substrates) only:

$$\boldsymbol{n}(\boldsymbol{r}) \;=\; (\cos\vartheta(z)\,\cos\varphi(z)\;;\;\cos\vartheta(z)\,\sin\varphi(z)\;;\;\sin\vartheta(z))$$

The Frank's free energy density f of the sample reads as

$$f(\vartheta,\,\vartheta',\,\varphi') = \tfrac{1}{2}\,K_1\cos^2\vartheta(\vartheta')^2 + \tfrac{1}{2}\,K_2\,[\cos^4\vartheta(\varphi')^2 - 2\,q\cos^2\vartheta\varphi' + q^2] + \tfrac{1}{2}\,K_3\,[\,\sin^2\vartheta(\vartheta')^2 \;+\; \sin^2\vartheta\cos^2\vartheta(\varphi')^2]. \tag{1}$$

Here ϑ' and φ' denote the first z-derivatives, K_1, K_2 and K_3 are the elastic moduli, while $q = 2\pi/P$ is the twisting power and P is the pitch. The functions $\vartheta(z)$ and $\varphi(z)$ minimizing Eq. (1) are searched for by variational calculus using the Euler-Lagrange equations

$$\frac{\partial f}{\partial \vartheta} - \nabla_z \frac{\partial f}{\partial \vartheta'} = 0\,, \tag{2}$$

$$\frac{\partial f}{\partial \varphi} - \nabla_z \frac{\partial f}{\partial \varphi'} = 0\,. \tag{3}$$

Optics EXPRESS

As f does not depend on φ, Eq. (3) can immediately be integrated yielding

$$\varphi' = \frac{K_2 q}{(K_2 \cos^2\vartheta + K_3 \sin^2\vartheta)} \quad . \tag{4}$$

Here the integration constant was chosen as 0, in order to prevent divergence of φ' at the homeotropic boundary. Eq. (4) readily shows that the twisting power of the cholesteric is changing, if the director tilts away from the planar state. As $K_2 < K_3$, a reduction of the twisting power occurs corresponding to the K_2/K_3 ratio, as one moves from the planar toward the homeotropic boundary.

Multiplying Eq. (2) with ϑ', it can be transformed into a total differential

$$\nabla_z\{K_1 \cos^2\vartheta(\vartheta')^2 + K_3 \sin^2\vartheta(\vartheta')^2 - K_2 \cos^4\vartheta(\varphi')^2 + 2\,K_2\,q \cos^2\vartheta\varphi' - K_3 \sin^2\vartheta\cos^2\vartheta(\varphi')^2\} = 0.$$

After substituting φ' from Eq. (4) the integration yields

$$(\vartheta')^2 = \frac{B - \frac{K_2^2 q^2 \cos^2\vartheta}{(K_2\cos^2\vartheta + K_3\sin^2\vartheta)}}{(K_1\cos^2\vartheta + K_3\sin^2\vartheta)} \quad . \tag{5}$$

The inverse functions $z(\vartheta)$ and $\varphi(\vartheta)$ can then be derived as the integrals

$$z(\vartheta) = \int_{\vartheta_p}^{\vartheta} \frac{1}{\theta'} d\theta = \int_{\vartheta_p}^{\vartheta} \sqrt{\frac{(K_1\cos^2\theta + K_3\sin^2\theta)(K_2\,cos^2\theta + K_3\sin^2\theta)}{B\,(K_2\,cos^2\theta + K_3\sin^2\theta) - K_2^2\,q^2\cos^2\theta}}\, d\theta \tag{6}$$

$$\varphi(\vartheta) = \int_{\vartheta_p}^{\vartheta} \frac{\varphi'}{\theta'}\, d\theta = \int_{\vartheta_p}^{\vartheta} \frac{K_2 q}{(K_2\cos^2\theta + K_3\sin^2\theta)} \sqrt{\frac{(K_1\cos^2\theta + K_3\sin^2\theta)(K_2\cos^2\theta + K_3\sin^2\theta)}{B\,(K_2\cos^2\theta + K_3\sin^2\theta) - K_2^2\,q^2\cos^2\theta}}\, d\theta. \tag{7}$$

The integrals in Eqs. (6,7) can be calculated numerically. The integration constant B should first be iterated until the condition $z(\vartheta_h) = d$ fulfils. Then $\varphi_h = \varphi(\vartheta_h)$ provides the total twist angle of the director in the sample. In the formulas above, ϑ_p and ϑ_h correspond to the tilt angles at the planar and homeotropic boundaries, respectively. During the calculations, the material parameters of E7 were taken from the supplier as: $K_1 = 11.3 \times 10^{-12}$ N, $K_2 = 6.7 \times 10^{-12}$ N, $K_3 = 18.6 \times 10^{-12}$ N. Strong boundary conditions with a small pretilt angle ($\vartheta_p = 1°$and $\vartheta_h = 89°$) and rubbing along the x-axis ($\varphi_p = 0$) were assumed.

Figures 8(a) and 8(b) depict the numerically calculated $\vartheta(z)$ and $\varphi(z)$ dependences, respectively, for different values of the helical pitch P. It can clearly be seen that the twist angle decreases, while the tilt angle increases with the growth of the pitch. Moreover, the shape of the $\vartheta(z)$ curve changes from concave at the initial ($P = P_0$) to convex at the compensated (P $\rightarrow \infty$) state. The convexity of $\vartheta(z)$ in the compensated state is a direct consequence of the missing twist contribution ($q = 0$) in Eq. (5) and the $K_1/K_3 < 1$ ratio. The twist term at $q \neq 0$, mainly contributes and reduces ϑ' near the planar side, thus inducing the transition to concave shape at smaller P. At the same time, $\varphi(z)$ preserves convexity for all pitch values, as expected from Eq. (4).

The simulation results in Figs. 8(a)–8(b) show only the curves for various values of the *righ-handed* pitch. Note, however, that the $\vartheta(z)$ curve is not sensitive to the helical sense, as Eq. (5) contains q^2 only. Thus the $\vartheta(z)$ curves belonging to *right-handed* and *left-handed* helices of the same $|P|$ should coincide. In contrast to that, the sign of $\varphi(z)$ depends on the helical sense as seen from Eq. (4); thus the $\varphi(z)$ curves of *left-handed* helices can be obtained by reflecting the $\varphi(z)$ curves of *right-handed* ones onto the horizontal axis.

Optics EXPRESS

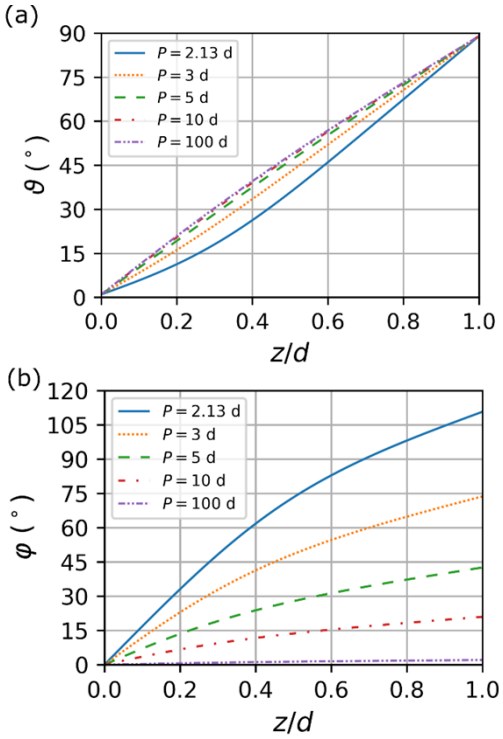

Fig. 8. Director profile across the sample for different values of the pitch P. (a) The tilt angle $\vartheta(z)$, (b) the azimuthal angle $\varphi(z)$.

4.2. *Evolution of the pitch under the UV field*

Due to the photo-induced chirality effect of chiral dopant M5(R), the pitch $P(I_{\mathrm{uv}})$ of the sample could change in spatially homogeneous manner, when the sample was submitted to uniform UV intensity.

In a usual planar geometry, with the helical axis perpendicular to the substrates, an integer number of half turns must be formed in the sample due to the boundary conditions (Grandjean-texture), i.e. the pitch can take only discrete values [11,19]. In the HAC geometry used in our experiments, however, $P(I_{\mathrm{uv}})$ could be tuned freely by the UV intensity I_{uv}, due to the lack of azimuthal constraint on the director at the homeotropic surface. Moreover, due to the large pitches involved, the sample manifested as a slightly twisted system. Consequently, the total twist angle $\varphi_h(I_{uv}) = \varphi(z = d)$ changed smoothly depending on the small ratio of $d/P(I_{\mathrm{uv}})$ [12,20].

According to the UV intensity dependence of $P(I_{\mathrm{uv}})$ [11], we distinguished two intensity regions separated by the critical intensity I_{c} : ① In the low UV intensity region of $0 < I_{\mathrm{uv}} < I_{\mathrm{c}}$, the handedness of the helical structure was the same as that in the unilluminated ($I_{\mathrm{uv}} = 0$) state. Increasing I_{uv} resulted in the enlargement of the pitch $|P(I_{\mathrm{uv}})|$, and hence in diminishing φ_h. ② At $I_{\mathrm{uv}} = I_{\mathrm{c}}$, one had a compensated cholesteric structure, where there is no twist of the director and hence $\varphi_h = 0$. ③ In the high UV intensity region of $I_{\mathrm{c}} < I_{\mathrm{uv}}$, the handedness experienced a reversal, while $|P(I_{\mathrm{uv}})|$ decreased and $|\varphi_h|$ increased accordingly with growing I_{uv}. Thus, the rotation of $\varphi_h(I_{uv})$ at the border of the low and the high intensity regions was monotonic and smooth.

Optics EXPRESS

4.3. Characteristics of the transmitted light

In Fig. 6(b), we have seen that a smaller rotation of the polarization corresponded to a higher *DoLP* of the transmitted beam. Similarly, Fig. 7 depicts that in a thicker cell one finds a higher *DoLP*. These two observations fully coincide with the expectations from the Mauguin theorem for light transmission in twisted liquid crystal systems, which predicts an optical waveguiding mode (rotation of the light polarization with the director) if the condition $2\ \pi\ \Delta n\ d/\lambda \gg \varphi_h$ is satisfied [21]. One has to take into account, however, that the hybrid aligned structure may cause complications, as the increasing tilt angle reduces the effective optical anisotropy (Δn in the above formula) and hinders the fulfilment of the Mauguin condition near the homeotropic substrate.

To explore the consequences of the twisted hybrid aligned director structure, characteristics of the transmitted light have numerically been simulated using the Jones-matrix method [3,22]. To calculate the Jones-matrix of the cell, we split it into thin slabs of thickness dz along the z-direction. If dz is small enough, the twist and tilt angles can be regarded constant in a slab with a good approximation. Each slab is then a birefringent waveplate with a retardation $\Delta\Phi_i$ and the direction of its slow axis at the angle φ_i with respect to the x-axis. The retardation for the ith slab coming from its birefringence can be calculated as

$$\Delta\Phi_i = \frac{2\pi}{\lambda}\left(n_e\left(1+\frac{n_e^2-n_o^2}{n_o^2}\sin^2\vartheta_i\right)^{-1/2} - n_o\right)dz, \tag{8}$$

where λ is the wavelength of light, n_o and n_e are the ordinary and extraordinary refractive indices, respectively, while ϑ_i is the tilt angle of the director at the position of the ith slab. Let us denote the Jones-matrix of the ith slab of the liquid crystal cell as $\mathbf{M}_{\mathrm{wp}}(\varphi_i, \Delta\Phi_i)$ [22]. Assuming an input light polarized along the x-axis with the Jones vector $\mathbf{J}_{in} = \begin{bmatrix} 1 \\ 0 \end{bmatrix}$, the Jones vector of the output light is calculated by $\mathbf{J}_{out} = \left(\prod_{i=1}^{n} \mathbf{M}_{wp}(\varphi_i, \Delta\Phi_i)\right)\mathbf{J}_{in}$, where the slab corresponding to $i\ = 0$ starts at $z\ = 0$, and the one with $i\ = n$ ends at $z\ = d$. By knowing J_{out}, the azimuth angle of the output light's polarization ellipse (α) and the degree of linear polarization (*DoLP*) can be given after straightforward calculations [22].

The refractive indices of E7 from supplier were $n_\mathrm{e} = 1.741$ and $n_\mathrm{o} = 1.517$. It was found that the outgoing light is nearly linearly polarized, though it possesses a small ellipticity. The direction of the polarization (i.e. the direction of the slow axis of the ellipse) makes an angle α with the x axis, with α being slightly smaller than the maximal twist angle φ_h, as illustrated in Fig. 9(a). Our simulations agree well with the experiments. The rightmost end of the simulated data in Fig. 9(a) corresponds to the smallest pitch ($P_0 = 2.13\ d$), which was actually used in the experiments. The difference between the simulated and the measured value ($\approx 90°$) of α is less than 15°, which is plausible since we used the elastic constants and refractive indices of the pure nematic E7 in the simulation, not taking into account the changes in the material parameters caused by the photosensitive dopant. Little adjustment of the material constants, e.g. either purely decreasing K_2 by about 19% or purely increasing K_3 by 23% leads to $\alpha \approx 90°$.

One expects that the transmitted light will become more linearly polarized at smaller d/P. Surprisingly, the ellipticity does not vary monotonically with the pitch; instead it exhibits a damped oscillation upon enlarging P, as depicted in Fig. 9(b). This behavior reminds to that of the thickness dependence of the transmission of a twisted nematic cell [23,24]. Note that theoretically, at normal incidence, *DoLP* depends on the angles ϑ and $|\varphi|$, i.e. it should not be sensitive to the sign of the pitch. Nevertheless, the experiment shown in Fig. 6(b) depicts a slight asymmetry. It can be attributed to UV light induced change of the material parameters (e.g. elastic moduli) or slight misalignment of the optical setup.

Optics EXPRESS

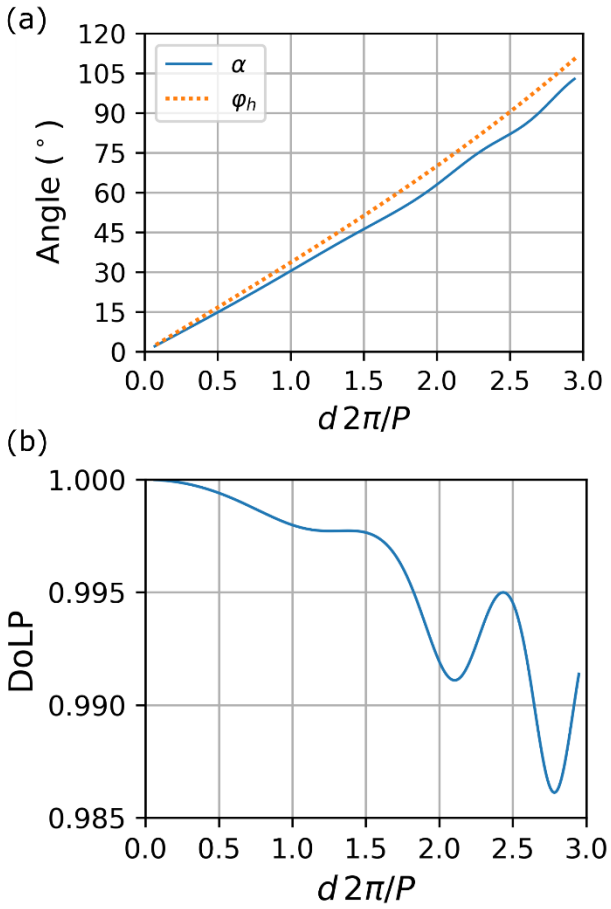

Fig. 9. (a) Comparison of the total twist angle $\varphi_h = \varphi(z = d)$ and the azimuth angle of the output light's polarization ellipse (α) as a function of the thickness to pitch ($d\ 2\pi/P$) ratio. (b) The degree of linear polarization (*DoLP*) versus $d\ 2\pi/P$. The simulation was performed at fixed $d = 60\ \mu$m.

As a conclusion, under the photo-tuning operation, the cholesteric sample forms an optical waveguiding structure; thereby the transmitted beam becomes a guided-wave, even when the pitch and the chirality of sample varies with I_{uv}. Consequently, our device acted as a polarization rotator that allowed the transmitted beam to be linearly polarized with a fixed intensity and controlled polarization direction.

4.4. Response time of the polarization changes

As we described earlier [11], the UV illumination induces a conformational transition of the chiral dopant to an excited state, which possesses a different sign of its helical twisting power. This excited conformer returns to its initial, unexcited state via thermal relaxation. Therefore, in order to ensure a desired rotation angle of the light polarization, illumination by a proper UV intensity should permanently be maintained.

Figure 10 exhibits an example of how the polarization angle α behaves upon UV intensity transients. It can be figured out that our sample responded with a response time of about 15 minutes, both on switching the UV on or off. One can identify at least two different mechanisms, which determine the response times: (a) the conformational transitions of the dopants and (b) the

Optics EXPRESS

adjustment of the director structure corresponding to the altered value of the pitch. We assume that the molecular processes (excitation by UV light and the thermal back relaxation) occur at a shorter time scale, so the response time is basically governed by the director relaxation time which is proportional to the square of the sample thickness. This assumption is supported by the fact that former measurements on the light induced rotation of electroconvection patterns (which reflect the underlying rotation of the director) in $d = 6\,\mu m$ thick samples (in contrast to the $d = 60\,\mu m$ used here) yielded a response time in the order of a few seconds [11].

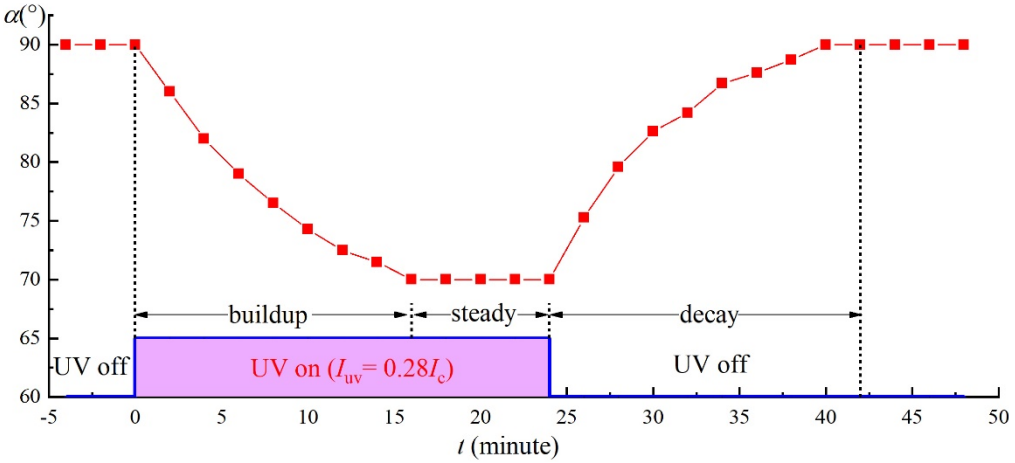

Fig. 10. Temporal variation of the polarization angle upon switching the UV illumination on and off.

We note that the reason of using large sample thickness was our aim to realize polarization rotation with large *DoLP*. Reducing the sample thickness in order to speed up the device at the same concentration of the dopant would constrain the range of the polarization rotation angle to lower values. If the angle range has to be maintained, the dopant concentration has to be increased (as was done for the samples shown in Fig. 7) in order to shorten the pitch, but then the Mauguin condition might be less fulfilled, increasing the ellipticity of the transmitted beam. Thus, we conclude that having large *DoLP* (≈ 1) and fast response implies contradictory requirements.

5. Conclusion

We reported that the output polarization state of light can be manipulated continuously by applying a UV field, depending on the intensity of the uniform UV illumination.

In addition to the *continuous rotation* of the linear polarization, where the rotation angle could sweep the whole horizontal plane ($-\pi/2 \sim\leq \alpha \leq +\pi/2$) for the transmitted beam, it should be stressed that our prototype could work in a *dynamical manner*. It is based on bulk effect of the self-assembled helical structure being either compressed or dilated in response to the strength of the controlling UV field. In contrast, conventional linear polarization rotators only perform inflexibly, as are usually based on surface effects, where the surface alignments have been permanent since the devices were fabricated [25,26].

Funding. Hungarian National Research (NKFIH FK142643); Guangdong Provincial Science and Technology Plan (2022A0505050072, 2022A1515010777); Grantová Agentura České Republiky (22-16499S); National Key Research and Development Program of China (2020YFE0100200); Guangzhou Science and Technology Program key projects (202201000008); Fundamental Research Funds for the Central Universities (2023FRFK06011); Magyar Tudományos Akadémia (22-16499S); Guangdong Provincial Key Laboratory of Optical Information Materials and Technology (2017B030301007).

Optics EXPRESS

Acknowledgments. This work was supported by Guangdong Provincial Science and Technology Plan (2022A15150 10777 and 2022A0505050072); Hungarian National Research, Development, and Innovation Office under Grant NKFIH FK142643, EIG CONCERT-Japan project FerroFluid (2023-1.2.1-ERA_NET-2023-00008); Czech project, Czech Science Foundation (22-16499S); National Key R&D Program of China (2020YFE0100200), Science and Technology Projects in Guangzhou (202201000008) and Guangdong Provincial Key Laboratory of Optical Information Materials and Technology (2017B030301007); Fundamental Research Funds for the Central Universities (2023FRFK06011). P.S. was supported by the János Bolyai Research Scholarship of the Hungarian Academy of Sciences.

Disclosures. The authors declare no conflicts of interest.

Data availability. Data underlying the results presented in this paper are not publicly available at this time but may be obtained from the authors upon reasonable request.

References

1. V. G. Chigrinov, V. M. Kozenkov, and H. Kwok, *Photoalignment of Liquid Crystalline Materials: Physics and Applications* (John Wiley & Sons, Ltd., 2008).
2. W. Hu, A. Srivastava, F. Xu, *et al.*, "Liquid crystal gratings based on alternate TN and PA photoalignment," Opt. Express **20**(5), 5384–5391 (2012).
3. D.-K. Yang and S.-T. Wu, *Fundamentals of Liquid Crystal Devices* (John Wiley & Sons Ltd, 2006).
4. S.-T. Wu and D.-K. Yang, *Reflective Liquid Crystal Displays* (John Wiley & Sons, Ltd, 2001).
5. H. Ren and S. T. Wu, "Liquid-crystal-based linear polarization rotator," Appl. Phys. Lett. **90**(12), 121123 (2007).
6. T.-Y. Chung, M.-C. Tsai, C.-K. Liu, *et al.*, "Achromatic linear polarization rotators by tandem twisted nematic liquid crystal cells," Sci Rep **8**(1), 13691 (2018).
7. M. Honma, K. Okitsu, and T. Nose, "Reflective liquid crystal polarization rotator with ultraviolet- polymerizable liquid crystal retardation film," Jpn. J. Appl. Phys. **52**(2R), 022501 (2013).
8. M. J. Abuleil and I. Abdulhalim, "Tunable achromatic liquid crystal waveplates," Opt. Lett. **39**(19), 5487–5490 (2014).
9. M. Schadt and M. Stalder, "Linearly polarized light with axial symmetry generated by liquid-crystal polarization converters," Opt. Lett. **21**(23), 1948–1950 (1996).
10. J. Sun, L. Yu, L. Wang, *et al.*, "Optical intensity-driven reversible photonic bandgaps in self-organized helical superstructures with handedness inversion," J. Mater. Chem. C **5**(15), 3678–3683 (2017).
11. H. Jing, Y. Xiang, M. Xu, *et al.*, "Light-Controllable Electroconvection Patterns in a Chiral Nematic Liquid Crystal," Phys. Rev. Appl. **10**(1), 014028 (2018).
12. Y. Xiang, H. Jing, H. Chen, *et al.*, "Light-driven rotation of gratings formed by electroconvection patterns in cholesteric liquid crystals," J. Mol. Liq. **337**, 116366 (2021).
13. A. S. Abdullaev, D. A. Kostikov, M. N. Krakhalev, *et al.*, "Complete light polarization control using a chiral-nematic cell with tangential-conical boundary conditions," Opt. Mater. **146**, 114521 (2023).
14. G. Nava, R. Barboza, F. Simoni, *et al.*, "Optical control of light polarization in heliconical cholesteric liquid crystals," Opt. Lett. **47**(12), 2967–2970 (2022).
15. G. Nava, F. Ciciulla, O. S. Iadlovska, *et al.*, "Pitch tuning induced by optical torque in heliconical cholesteric liquid crystals," Phys. Rev. Res. **1**(3), 033215 (2019).
16. T. Orlova, F. Lancia, C. Loussert, *et al.*, "Revolving supramolecular chiral structures powered by light in nanomotor-doped liquid crystals," Nat. Nanotechnol. **13**(4), 304–308 (2018).
17. R. Eelkema, M. M. Pollard, N. Katsonis, *et al.*, "Rotational reorganization of doped cholesteric liquid crystalline films," J. Am. Chem. Soc. **128**(44), 14397–14407 (2006).
18. H. Wu, W. Hu, H. Hu, *et al.*, "Arbitrary photo-patterning in liquid crystal alignments using DMD based lithography system," Opt. Express **20**(15), 16684–16689 (2012).
19. P. G. de Gennes and J. Prost, *The Physics of Liquid Crystals* (Oxford University Press, 1993).
20. P. Z. Sun, Z. Liu, W. Wang, *et al.*, "Light-reconfigured waveband-selective diffraction device enabled by micro-patterning of a photoresponsive self-organized helical superstructure," J. Mater. Chem. C **4**(39), 9325–9330 (2016).
21. T. Scharf, *Polarized Light in Liquid Crystals and Polymers* (John Wiley & Sons, 2007).
22. D. S. Kliger, J. W. Lewis, and C. Einterz, *Randall, Polarized Light in Optics and Spectroscopy* (Academic Press, 1990).
23. C. H. Gooch and H. A. Tarry, "Optical characteristics of twisted nematic liquid-crystal films," Electron. Lett. **10**(1), 2–4 (1974).
24. C. H. Gooch and H. A. Tarry, "The optical properties of twisted nematic liquid crystal structures with twist angles ⩽90 degrees," J. Phys. D: Appl. Phys. **8**(13), 1575–1584 (1975).
25. C. Y. Huang, H. Y. Tsai, Y. H. Wang, *et al.*, "Linear polarization rotators based on dye-doped liquid crystal cells," Appl Phys Lett **96**(19), 191103 (2010).
26. Y. Xiang, H. Jing, W. Sun, *et al.*, "Topological defects arrays and control of electro-convections in periodically photo-aligned bent-core nematics," J. Mol. Liq. **318**, 114058 (2020).